EFDA–JET–CP(10)08/27

J. Mailloux, X. Litaudon, P.C. de Vries, J. Garcia, I. Jenkins, B. Alper, Yu. Baranov, M. Baruzzo, M. Beurskens, M. Brix, P. Buratti, G. Calabro, R. Cesario, C.D. Challis, K. Crombe, O. Ford, D. Frigione, C. Giroud, M. Goniche, N. Hawkes, D. Howell, P. Jacquet, E. Joffrin, V. Kiptily, K.K. Kirov, P. Maget, D.C. McDonald, V. Pericoli-Ridolfini, V. Plyusnin, F. Rimini, M. Schneider, S. Sharapov, C. Sozzi, I. Voitsekovitch, L. Zabeo and JET EFDA contributors

Towards a Steady-State Scenario with ITER Dimensionless Parameters in JET

Towards a Steady-State Scenario with ITER Dimensionless Parameters in JET

J. Mailloux[1], X. Litaudon[2], P.C. de Vries[3], J. Garcia[2], I. Jenkins[1], B. Alper[1], Yu. Baranov[1], M. Baruzzo[4], M. Beurskens[1], M. Brix[1], P. Buratti[5], G. Calabro[5], R. Cesario[5], C.D. Challis[1], K. Crombe[6], O. Ford[1], D. Frigione[5], C. Giroud[1], M. Goniche[2], N. Hawkes[1], D. Howell[1], P. Jacquet[1], E. Joffrin[2], V. Kiptily[1], K.K. Kirov[1], P. Maget[2], D.C. McDonald[1], V. Pericoli-Ridolfini[5], V. Plyusnin[7], F. Rimini[9], M. Schneider[2], S. Sharapov[1], C. Sozzi[8], I. Voitsekovitch[1], L. Zabeo[1] and JET EFDA contributors*

JET-EFDA, Culham Science Centre, OX14 3DB, Abingdon, UK

[1]EURATOM-CCFE Fusion Association, Culham Science Centre, OX14 3DB, Abingdon, OXON, UK
[2]CEA, IRFM, F-13108 Saint-Paul-lez-Durance, France
[3]FOM Rijnhuizen, Association EURATOM-FOM, Netherlands
[4]Consorzio RFX, EURATOM-ENEA sulla Fusione, 35137 Padova, Italy,
[5]Associazione EURATOM-ENEA sulla Fusione, C.R. Frascati, Roma, Italy
[6]Department of Applied Physics UG (Ghent University) Rozier 44 B-9000 Ghent Belgium,
[7]Associação EURATOM/IST, Instituto de Plasmas e Fusão Nclear, Lisbon, Portugal
[8]Instituto di Fisica del Plasma CNR, EURATOM-ENEA-CNR Association, Milano, Italy
[9]EFDA-CSU, Culham Science Centre, OX14 3DB, Abingdon, OXON, UK
** See annex of F. Romanelli et al, "Overview of JET Results",*
(23rd IAEA Fusion Energy Conference, Daejon, Republic of Korea (2010)).

Preprint of Paper to be submitted for publication in Proceedings of the
23rd IAEA Fusion Energy Conference, Daejon, Republic of Korea
(10th October 2010 - 16th October 2010)

ABSTRACT

To demonstrate ITER Steady-State scenario, total $\beta_N \approx 3$, thermal $\beta_N \approx 2.4$, $H_{98} \approx 1.4$-1.5 and bootstrap current fraction (f_{BS}) 7≥50% need to be demonstrated in existing devices, ideally at dimensionless parameters such as the normalised Larmor radius (ρ^*), collisionality (ν^*), ratio of ion to electron temperature (T_i/T_e), qprofile and Mach number as close as possible to those in ITER since they affect transport and/or current drive. This motivated experiments in JET where the performance of high triangularity NBI-only plasmas developed to study stability and confinement at high β_N and H_{98} was extended to higher B_T, I_P (2.7T, 1.8MA, $q_{95} = 4.7$) and power (electron heating ICRH, LHCD in addition to NBI). Good ICRF coupling is obtained with gas dosing, with good edge confinement ($H_{98} \sim 1$) and type I ELMs. With the ICRF ELM resilient systems, up to 8MW is coupled. LH coupling is affected by the nearest ICRH antenna and only $P_{LH} \approx 2.5$MW was available. The following steady (>10× τ_E) and peak performances are obtained: $H_{98} \approx 1.2$ (up to 1.35), $\beta_N \approx 2.7$ (up to 3.1). The thermal fraction is up to 80% and $\langle T_i \rangle / \langle T_e \rangle \approx 1.05$, with $T_e = T_i$ at the pedestal. The Mach number at midradius ≈ 0.3, and ρ^*/ρ^*ITER ≈ 2, ν^*/ν^*ITER ≈ 4. In the range of target q-profiles used ($1.8 < q_{min} < 2.9$), only plasmas with an internal transport barrier, in addition to an edge transport barrier, have $H_{98} > 1.1$. In some shots, n = 1 kink modes are seen, often limiting the performance and in a few cases causing disruptions. In all shots the q-profile is evolving, indicating a shortage of Non-Inductive (NI) current. Interpretative modelling show that $f_{BS} \approx 40$-45% where the highest f_{BS} is for plasmas with highest q_0 and β_N. Predictive modelling shows that f_{BS} goes from 45% to 50% when scaling to ITER ν^*. NBI provides ~20% of externally driven NI current and LHCD contributes <10%. An ECRH system was recently proposed for JET. Predictive modelling shows that ECCD can provide the narrow off-axis current required to maintain the q-profile at the time of high performance.

1. INTRODUCTION

ITER Steady-State (SS) scenario must have 7 50% bootstrap current fraction (f_{BS}), high normalised beta, total $\beta_N \approx 3$ and thermal $\beta_N \approx 2.4$, and $H_{98} \approx 1.4$-1.5 [1], where with $\beta_N = \beta_T aB/I_P$ with $\beta_T = 2\mu_0 p/B^2$, a = minor radius, B = magnetic field, I_P = plasma current and p = plasma pressure, and H_{98} is the energy confinement time normalised to the IPB98(y,2) scaling [2]. These conditions have been reached in existing devices, see for example [3]. However, it is important to demonstrate this in plasmas with dimensionless parameters such as the normalised Larmor radius (ρ^*), collisionality (ν^*), ratio of ion to electron temperature (T_i/T_e) and normalised rotation as close as possible to those expected in ITER, since they affect transport and/or current drive. This motivated dedicated experiments in JET at 2.7T/1.8MA, i.e. the highest B_T and I_P where high β_N is accessible with the present heating power available. Using Neutral Beam Ion (NBI) heating, Ion Cyclotron Radio Frequency (ICRF) and Lower Hybrid (LH) wave heating, and integrating recent JET scenario development advances [4],[5], and technical upgrades, this produced plasmas with steady (i.e. for times > 10×τ_E) $H_{98} = 1.2$, total and thermal β_N of 2.7 and 2.0 respectively, $\langle T_i \rangle / \langle T_e \rangle = 1.05$, $f_{BS} = 40\%$ at global ρ^*/ρ^* ITER ≈ 2, ν^*/ν^* ITER ≈ 4, achieved simultaneously for the first time.

2. OPTIMISATION FOR HIGH FREQUENCY WAVE COUPLING AND ITER-LIKE WALL COMPATIBILITY

To use the full heating and current drive capability in JET, these experiments rely on optimising the edge for HF wave coupling while maintaining good core and edge confinement. With a small amount of gas dosing (4×10^{21} e/s to 7.4×10^{21} e/s, D_2 + 10%H), suitable ICRF coupling is obtained while retaining good edge confinement ($H_{98} \approx 1$ for plasmas without Internal Transport Barrier (ITB)) with type I ELMs. With the new ICRF ELM resilient systems [6], PICRF up to 8MW is coupled (42MZ, H minority heating scheme). This resulted in a lower $<T_i>/<T_e>$, from 1.3 on shots with NBI only, to 1.05 on shots with highest P_{ICRF}. As observed in other experiments [7], LH coupling is degraded when the neighbouring ICRF antenna is powered. Good LH coupling (reflection coefficient <6% across all rows) was obtained for gas dosing > 6.2×10^{21} e/s, but such amounts were used only on a few shots, and typically P_{LH} = 2.5MW in the experiments described here, with parallel refractive index $N_{//}$ = 1.8 or 2.3. The high triangularity (average $\delta = 0.4$) configuration recently developed and exploited at lower BT, IP [5] was used, with $q_{95} = 4.7$. The plasma was made more suitable for future operation with the planned JET ITERlike wall by increasing the density at the start of PNBI to maximise NBI absorption, although this means it is harder to control the q profile, and by moving the outer strike-point to a tile capable of bearing higher power loads, but with the consequence that this degrades the pumping. In addition, with the gas dosing the ELM size was reduced (energy per ELM decreased by ~ 40%). However, more work is required to make this scenario fully compatible with operation with a metal wall in JET. Figure 1 shows the evolution of Pulse No: 77895, with P_{NBI} = 22.5MW, P_{ICRH} = 6.6 MW, P_{LH} = 2.3MW.

3. HIGH PERFORMANCE AT DIMENSIONLESS PARAMETERS NEARER ITER VALUES

3.1 PERFORMANCE COMPARABLE TO THAT OF SHOTS AT LOWER BT, IP

In recent NBI-only, lower B_T, I^P experiments described in [4], [5], two favourable domains for high β_N, H_{98} operation were identified: $1 < q_0 < 1.5$, where $H_{98} = 1.35$ was achieved, and $q_0 \geq 2$, where $H_{98} = 1.25$. For the experiments described here, the second domain was selected in order to optimise the bootstrap current. The target q-profile, i.e. q at the start of the additional power (P_{ADD}), has weak negative or positive magnetic shear, with $1.8 < q_0 < 2.9$ (Fig.2), but most shots have target $q_0 \geq 2$. The q-profile is not sustained, and has relaxed to q_0 just above 1, with increased magnetic shear for $\rho_T > 0.6$ ($\rho_T = (f_N)0.5$ with f_N = normalised toroidal flux), by the end of P_{ADD}, for example for Pulse No: 77895 shown on Fig.2. To reach β_N 7 2.7, P_{ADD} > 26MW is necessary, and peak β_N = 3.1 is obtained with 31MW. Steady $H_{98} \approx 1.2$ is achieved, see figure 1 for example, similar to that at lower B_T, I_P. (Note that the contribution from the NBI and ICRH fast particles is removed when calculating H_{98} in this paper, however, unless otherwise indicated, the total β_N is quoted). The plasmas have good edge confinement, but the improved confinement leading to $H_{98} > 1$ is due to the presence of an ITB, as shown on figure 3, where the normalised ion temperature gradient scale length $R/L_{Ti} = R|\nabla T_i|/Ti$ is used to illustrate the strength of the ITB. An analysis based on the

kinetic profiles confirms that the energy from the pedestal does not change very much for these shots (Fig.4(a), and the improvement in H98 is due to an increase of energy from the core (Fig.4(b).

3.2 ITBS TRIGGERED AT Q = 2

Evidence for ITBs in these plasmas is seen most clearly in T_i, but also in T_e and n_e, for example in Pulse No: 77592, Fig.5(a-b). Figure 5-c) shows the ion thermal diffusivity, χ_i, from a TRANSP [8] interpretative run using the experimental T_i, T_e, n_e and Z_{eff} profiles and the target q profile (the q profile at later times is calculated in TRANSP). χ_i is reduced by 2 for normalised radius $\rho_T < 0.5$, to reach $\approx 1\times10^4$ cm^2/s (average for $\rho_T < 0.5$) during the ITB. Note however that ci remains well above the neoclassical prediction (calculated in TRANSP by NCLASS [9]), which is typical of the plasmas shown here. The energy contained in the pedestal changes little during that shot, and most of the additional energy comes from the core, with the percentage of the plasma energy from the core increasing from 62% before the ITB to 73% during the ITB. Shots with NBI only and NBI + gas dosing were performed to investigate the effect of adding gas, PICRH & PLH on the performances. Similar H98 are obtained, but with a higher fraction of the energy coming from the pedestal in the NBI only shot (see Pulse No: 77877 on Fig.4(b). Figure 6 shows that ci is the same for $\rho_T < 0.5$, but is for $\rho_T > 0.5$, compared to shots that have in addition gas and PICRH.

χ_i in several shots with an ITB, its start and location are correlated with the arrival of the $q = 2$ surface in the plasma, within error bars, see Figure 7 (a) for example. The q profile is calculated using MSE data, taking into account the kinetic profiles. In addition, on several pulses, MHD events, for example Alfven grand cascades occurring when integer q surface enters the plasma, or fishbone-like modes at $q = 2$, support the conclusion that the ITB, or at least its triggering, is related to the $q = 2$ surface in most shots. This correlation between ITB and q is reminiscent of the 'optimised shear' regimes observed in JET, see [10] and references therein, although the ITBs here are much weaker. In a very few cases the ITB is better correlated with the presence of negative shear (none of these plasmas have deeply negative magnetic shear at the time of the ITB, but some have weak negative shear, with $q_0/q_{min} < 1.2$). Predictions for ITER SS scenario usually assume that the presence of an ITB requires negative magnetic shear, however, as shown here and in past experiments, it is not a necessary condition. It is also worth noting that the electron density in the plasmas discussed here is significantly higher than that of JET ITB plasmas with low d in JET, especially at the pedestal, compare for example to the JET plasmas in [11], and [10].

3.3 PLASMAS WITH HIGHEST PRESSURE GRADIENT ARE LESS STABLE

The highest H_{98} and β_N (1.35 and 3.1 respectively) are obtained on shots with the strongest ITBs. However, these plasmas are not steady, and the performance is often momentarily interrupted by fishbone-like modes linked to $q = 2$, and is in some cases terminated by a neoclassical tearing mode, NTM, (generally a 2/1 mode). Several of the plasmas with $q = 2$ fishbones retain good performances, until either P_{ADD} decreases or the ITB disappears (for example Pulse No: 78052 on figure 8(b), or Pulse No: 77894 on Fig.7, as the favourable q profile is lost as described in [12]. The fishbone-like

mode often destabilises a kink-like mode accompanied by loss of energetic ions [13], followed by observation of impurity radiation increase [14]. In a few cases, this mode has led to a plasma disruption. Figure 8(a) shows that Pulse No: 78085, which has the highest peak performance, exhibits the q = 2 fishbones, and its performance is eventually terminated by a 5/2 mode that triggers a 2/1 mode. The global pressure gradient is known to affect the plasma stability [15], and, is likely to play a role in the plasmas described here, as adding an ITB (assuming same pedestal) results in an increased global pressure gradient. Figure 8 also shows the peaking factor ($p_{peak} = p_0/<p>$, where p_0 is the pressure in the core, and <p> is the volume averaged pressure. The thermal pressure is used here). The pressure profile becomes more peaked on Pulse No: 78085, as the ITB moves to a smaller radius and gets stronger (Fig.9), and by the time the 5/2 mode occurs, ppeak has reached 3.8. It is worth noting that, because these plasmas have a good pedestal, the pressure gradient, and in particular ppeak, is significantly smaller than that observed in past ITB plasmas at low δ, as already remarked in [4],[5]. As a consequence, higher β_N values can be reached and maintained. But ppeak alone is not sufficient to predict the plasma stability in this experiment. For example, Pulse No: 77895 has higher p_{peak} than Pulse No: 78052 at the same β_N, but no fishbone-like modes are triggered, indicating that other factors play a role, for example the q profile as predicted in [15] and similarly to what is observed in [4], or the fast particles. The stability of, and modes encountered in, the plasmas used for the SS scenario development in JET are described in more details in [16].

3.4 DIMENSIONLESS PARAMETERS NEARER ITER TARGET

The confinement scaling shows a strong dependence on the normalised Larmor radius (ρ*) [17], while the normalised collisionality (ν*) affects density peaking [18] and current drive [19], and may also play a role in transport, as shown in [17], [20]. In this experiment, the global $\rho^*/\rho^*_{ITER} \approx 2$, ν^*/ν^* ITER » 4 (calculated as defined in [2]). ITER n* and f_{GDL} can not be matched simultanously in JET, and preference was given to the latter in these experiments, because of the need to develop a scenario compatible with the ITER-like wall. The Greenwald fraction (f_{Gr}) = 0.6-0.65, with $n_e = 4\text{-}5\times10^{19} m^{-3}$. This contributed to the plasmas having a large thermal energy fraction, up to 80%. They also have T_e/T_i at the pedestal and over most of the plasma volume, with $<T_i>/<T_e> = 1.05\text{-}1.1$, i.e. the value expected in ITER, and worth noting since T_i/T_e affects the turbulent transport. The flow shear also affects transport, see for example [12] and references therein, so it interesting to note that the plasmas described here have a normalised rotation ≈ 20% to 40% lower than that for shots with NBI only, the lowest values being for lowest fraction of PNBI/PADD. For shots with NBI-only, the thermal Mach number $M_{TH} = 0.57$ in the core ($r \approx 0.2$) and $M_{TH} = 0.30$ just inside the pedestal ($\rho \approx 0.8$), where $M_{TH} = (m/e)^{0.5}\, \upsilon_\phi\, T^{-0.5}$ [21], with T the ion temperature in eV and υ_ϕ the toroidal rotation in m/s. The shots with in addition gas + ICRH + LHCD have 0.34 < MTH < 0.49 in the core (the highest values in that dataset are for plasmas with the strongest ITB), and $0.16 < M_{TH} <$ 0.24 just inside the pedestal.

4. NON-INDUCTIVE CURRENT DRIVE

In all shots there is evidence that the qprofile is evolving, indicating a shortage of Non-Inductive (NI) current. According to TRANSP interpretative modelling for selected shots with $\beta_N \geq 2.6$, f_{BS} = 36-45%, where the highest fBS is found for the plasmas with highest q_0 and β_N. The current profiles for Pulse No: 78085 show that the bootstrap current, j_{BS}, is well aligned, with most of the contribution at $0.2 < \rho < 0.5$, where the gradient due to the ITB is located, but with a significant contribution from the pedestal (Fig.10). TRANSP predictions using Sauter BS model [19] with equations parametrised in terms of ν_e^* and ν_i^*, show that f_{BS} increases from 45% to 50% when scaling to ITER ν^*, just making the minimum requirement. The NBI current, $j_{NBI} \approx 20\%$ of the total current, j_{TOT}, and is located on-axis. CRONOS [22], [23] calculations for shot 77895 show similar quantities and location for j_{BS} and j_{NBI} , although j_{BS} is slightly lower, 40% [24], due to the smaller gradient. This shot has in addition P_{LH} = 2.3MW with $N_{//} = 2.1$, and [24] finds that the LH current is $\approx 10\%$, located at $\rho \approx 0.6$. However, experimental observations, including from modulation experiments in similar shots as per method described in [25], indicate that this is likely to be an overestimation, and very little P_{LH} makes it past $\rho = 0.8$. This is at least in part because the accessibility for LH waves with $N_{//} = 1.8$ and 2.1 is marginal at the pedestal ne and BT of these experiments. Additionally, non-linear effects in the SOL layer may play a role [26], enhanced since the wave spends a longer time in the edge. Increasing B_T to 3.4T (with same q_{95}, i.e. I_P = 2.2MA) will improve wave accessibility, assuming ne,pedestal scales linearly with IP, as observed when going from 1.7T/1.15MA to 2.7T/1.8MA. To make these plasmas steady-state with the q-profile required for high performance would mean replacing the Ohmic current, j_{OHM}, by NI current. From figure 12-c), this means an additional NI current contribution at $0.4 < \rho < 0.6$. This is confirmed by CRONOS predictive calculations [24]. This location is also consistent with the need for 2/1 NTMs avoidance as shown in [4]. Recently, an ECRH system was proposed for JET [27]. Predictive CRONOS modelling with ECCD in this scenario indicates that it can provide the off-axis current required to sustain the q-profile favourable to the ITB and hence maintain the performance.

CONCLUSION

Through enhancements and dedicated experiments, JET has made further advance towards the conditions required for the ITER SS scenario, producing plasmas in which ITER-like values of the key dimensionless parameters bN total and thermal, H98(y,2), $\langle T_i \rangle / \langle T_e \rangle$ were simultaneously achieved, at reduced ρ^* and ν^* compared to plasmas at lower B_T (Fig.11). The planned JET NBI power upgrade will enable closer match to ρ^* and ν^* ITER values at A/cm^2 10^{19}m^{-3} kev high β_N. Additional off-axis externally driven and BS current are required to make these plasmas SS, at $0.4 < \rho < 0.6$.

ACKNOWLEDGEMENTS

This work, part-funded by the European Communities under the contract of Association between EURATOM and CCFE, was carried out within the framework of the European Fusion

Development Agreement. The views and opinions expressed herein do not necessarily reflect those of the European Commission. This work was also partfunded by the RCUK Energy Programme under grant EP/G003955.

REFERENCES

[1]. A. R. Polevoi et al, IAEA-CSP-19/C ISNN CT/P-08 Vienna (2003)
[2]. ITER PHYSICS BASIS EDITORS, Nuclear Fusion **39** (1999) 2175
[3]. E. Doyle et. al., Nuclear Fusion **50** (2010) 075005
[4]. C.D. Challis et al, 36th EPS Conf. on Plasma Phys. Sofia, 2009 ECA Vol.33E, P-5.172
[5]. F. Rimini et al., Proc. 22th IAEA conference, Geneva, 2008 ex_1-2
[6]. M.-L. Mayoral et al., 36th EPS Conf. on Plasma Phys. Sofia, 2009 ECA Vol.33E, O-4.048
[7]. K. Kirov et al., Plasma Physics and Controlled Fusion **51** (2009) 044003
[8]. R.J. Goldston et al, Journal of Computational Physics **43** (1981) 61
[9]. W. Houlberg, et al., Physics of Plasmas **4** (1997) 3231
[10]. C. Gormezano et al., Fusion Science and Technology **53** (2008) 958
[11]. X. Litaudon et al., this conference, EXC/P4-12
[12]. P. Mantica et al., this conference, EXC/P9-2
[13]. V. Kiptily et al., this conference, EXS/P7-01
[14]. V. Plyusnin et al., 11st TCM IAEA, Kiev, 2009
[15]. G. Huysmans et al., Nuclear Fusion **39** (1999)1489
[16]. P. Buratti et al., this conference, EXS/P5-02
[17]. T. Luce et al., Plasma Physics and Controlled Fusion **50** (2008) 043001
[18]. H. Weisen et al., Plasma Physics and Controlled Fusion **48** (2006) A457
[19]. O. Sauter et al., Physics of Plasmas vol. **6** (1999) no.7
[20]. E. Joffrin et al., this conference, EXC/1-1
[21]. P. C. de Vries et al., Nuclear Fusion **48** (2008) 065006
[22]. V. Basiuk et al., Nuclear Fusion **43** (2003) 822
[23]. J. F. Artaud et al.. Nuclear Fusion **50** (2010) 043001
[24]. J. Garcia et al., in Radio Frequency Power in plasma, edited by V. Bobkov and J.-M. Noterdaeme, AIP conference proceedings 1187, Melville, New York (2009) pp. 31-38
[25]. K. Kirov et al., Nuclear Fusion **50** (2010) 075003
[26]. M. Goniche et al., accepted for publication in Plasma Physics and Controlled Fusion
[27]. G. Giruzzi et al., this conference, FTP/P6-11

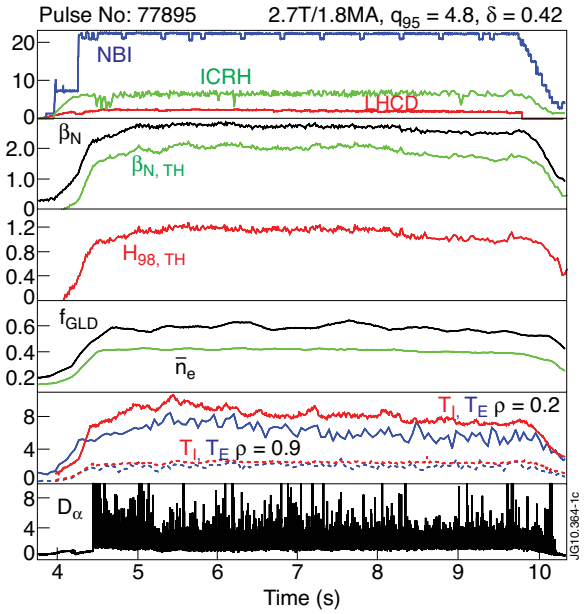

Figure 1: Evolution of Pulse No: 77895.

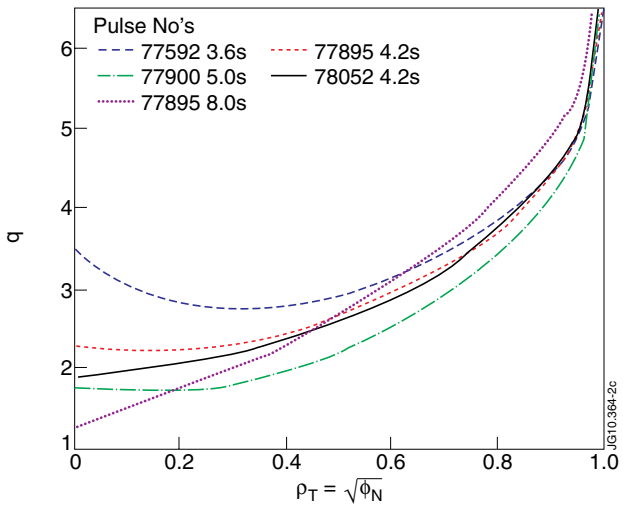

Figure 2: q profile at start of P_{ADD} for Pulse No's: 77592, 77895, 77900, 78052, and q profile at end of P_{ADD} for 77895.

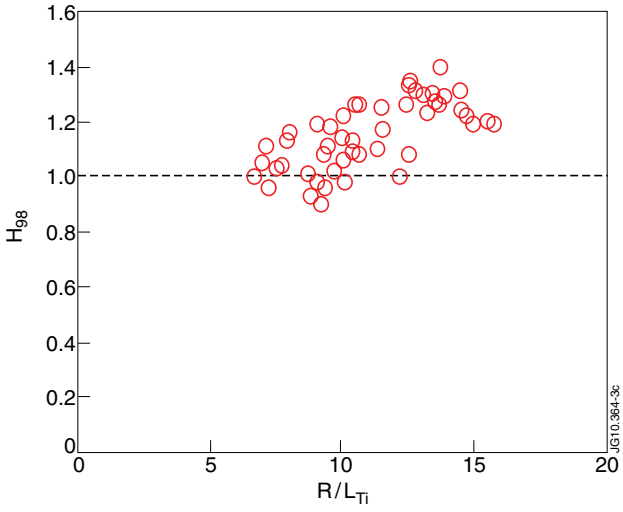

Figure 3: Peak H_{98} versus R/L_{Ti} for $\rho_T < 0.7$. Shots have 20MW < P_{ADD} < 32 MW and target q-profiles covering range of Fig.2

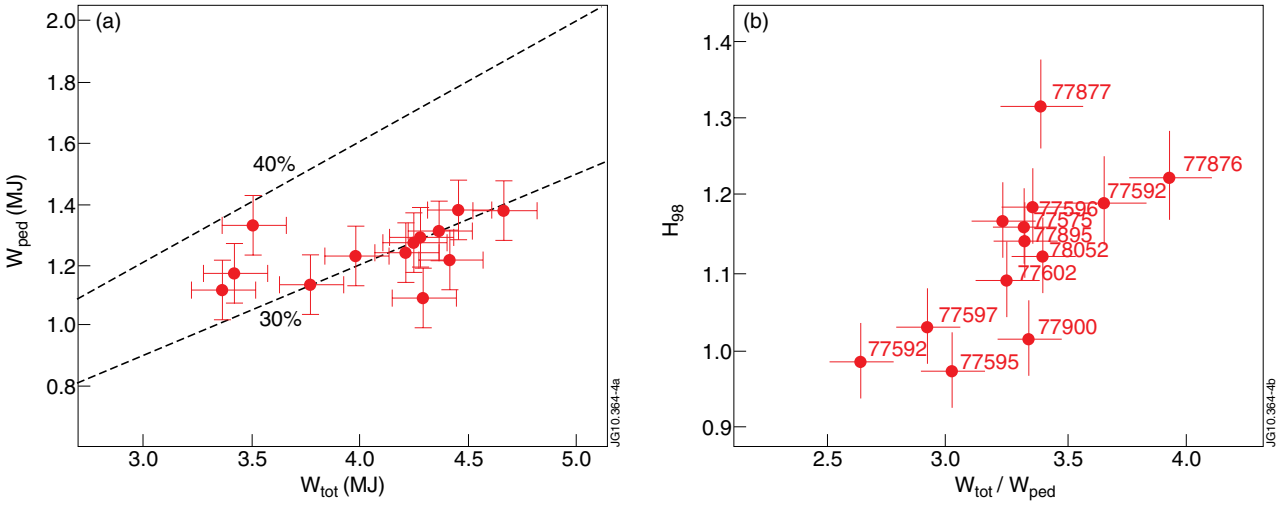

Figure 4 (a): energy from the pedestal as a function of the total energy, (b) H_{98} calculated from the kinetic profiles as a function of the ratio of total energy to pedestal energy.

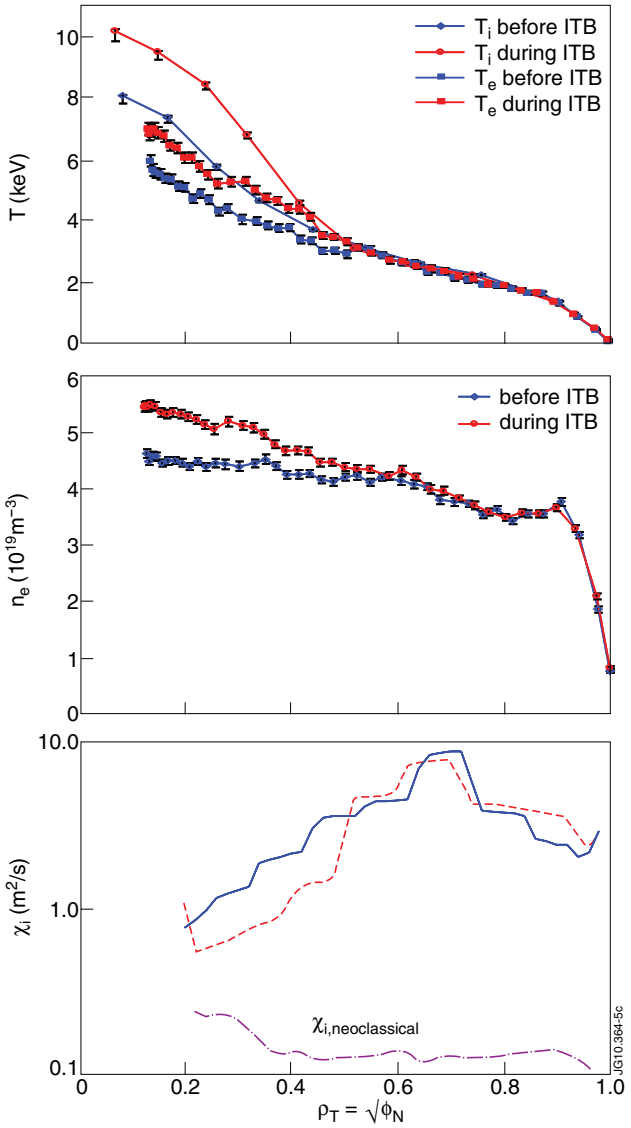

Figure 5: Profiles before (blue,5.4s-6.2s) and during (red, 7.8s-8.3s) ITB, for (a) n_e, (b) T_i (circles) and T_e (squares) and (c) χ_i from TRANSP, compared to neoclassical χ_l.

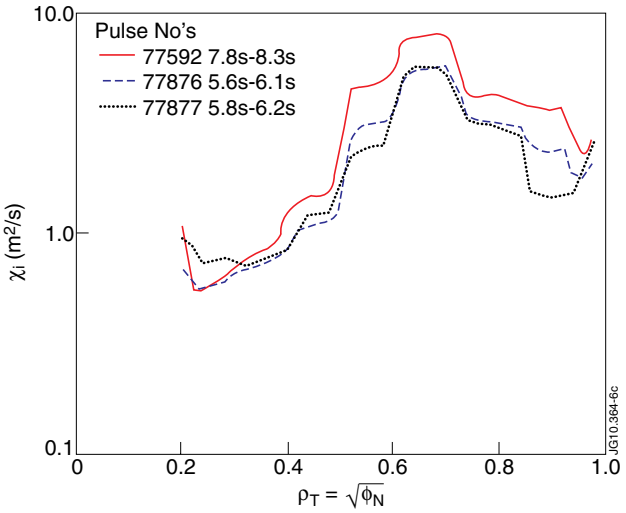

Figure 6: χ_i calculated by TRANSP for Pulse No's: 77876, NBI + gas, 77877, NBI only, and 77592, NBI + ICRH + gas.

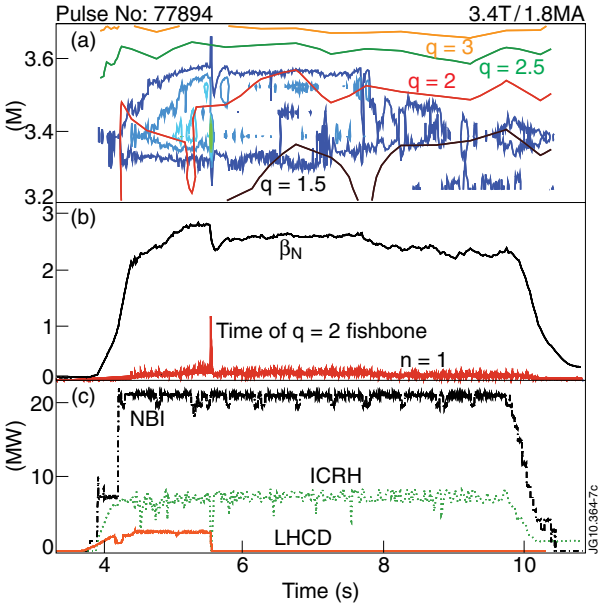

Figure 7: evolution of Pulse No: 77894 with a)Radial location of q and T_i normalised gradient surfaces, b)β_N and n = 1, c)P_{ADD}

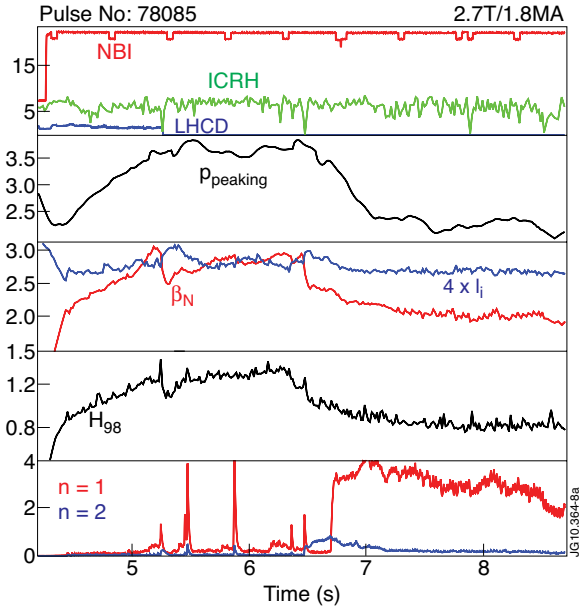

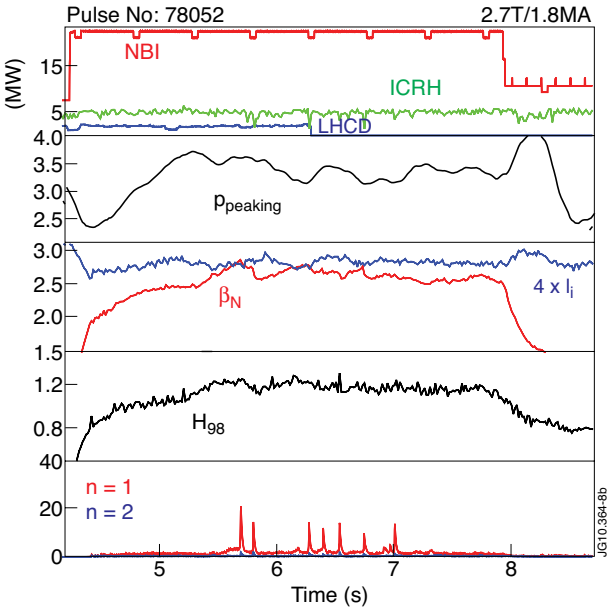

Figure 8. Evolution of Pulse No's: 78085 and 78052

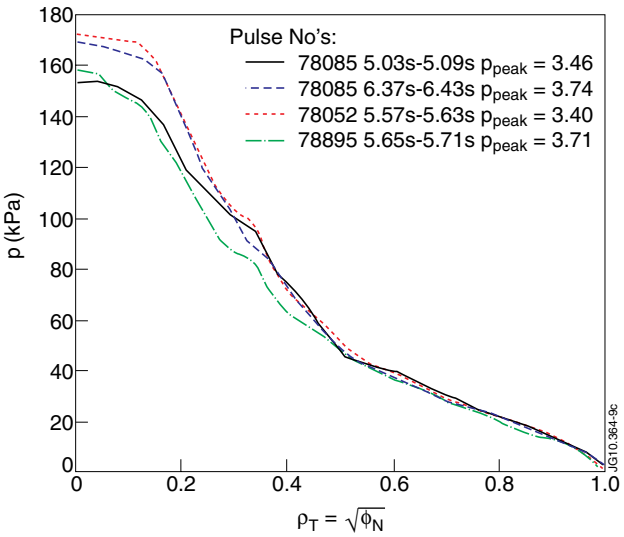

Figure 9: Pressure profiles for Pulse No's:78085, 78052 and 77895 at times of best performance.

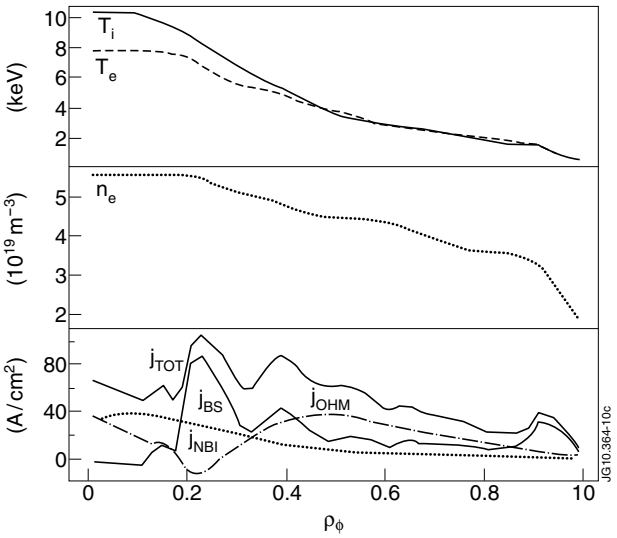

Figure 10: Profiles for Pulse No's: 78085 averaged over 5.4s-6.4s a) T_i, T_e, b) n_e, c) j_{TOT}, j_{Ohmic}, j_{NBI} and j_{BS} from TRANSP(there is no P_{LH} at that time).

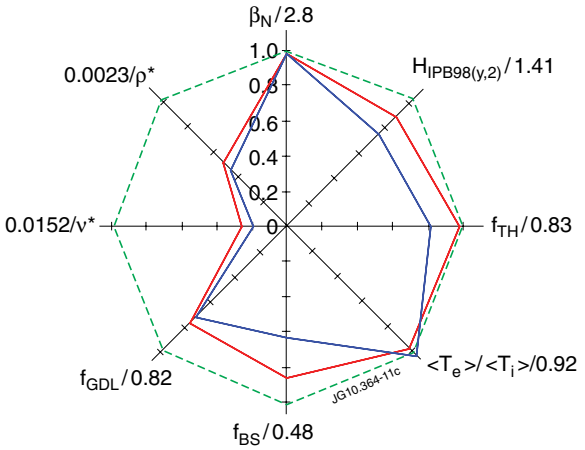

Figure 11. Dimensionless parameters for Pulse No: 78052 2.7T/1.8MA (red) normalised to ITER SS targets [1], compared to 70069 2.3T/1.5MA (blue) from [5].